AIP | Applied Physics Letters

Stress-mediated magnetoelectric control of ferromagnetic domain wall position in multiferroic heterostructures

Théo Mathurin, Stefano Giordano, Yannick Dusch, Nicolas Tiercelin, Philippe Pernod, and Vladimir Preobrazhensky

Citation: Applied Physics Letters **108**, 082401 (2016); doi: 10.1063/1.4942388
View online: http://dx.doi.org/10.1063/1.4942388
View Table of Contents: http://scitation.aip.org/content/aip/journal/apl/108/8?ver=pdfcov
Published by the AIP Publishing

Stress-mediated magnetoelectric control of ferromagnetic domain wall position in multiferroic heterostructures

Théo Mathurin,[1] Stefano Giordano,[1,a)] Yannick Dusch,[1] Nicolas Tiercelin,[1] Philippe Pernod,[1] and Vladimir Preobrazhensky[1,2]
[1]*Joint International Laboratory LICS/LEMAC: IEMN, UMR CNRS 8520, ComUE Lille Nord de France, ECLille, Avenue Poincaré, BP 60069, 59652 Villeneuve d'Ascq, France*
[2]*Wave Research Center, Prokhorov General Physics Institute, Russian Academy of Science, 38 Vavilov str., Moscow 119991, Russia*

(Received 12 January 2016; accepted 6 February 2016; published online 22 February 2016)

The motion of a ferromagnetic domain wall in nanodevices is usually induced by means of external magnetic fields or polarized currents. Here, we demonstrate the possibility to reversibly control the position of a Néel domain wall in a ferromagnetic nanostripe through a uniform mechanical stress. The latter is generated by an electro-active substrate combined with the nanostripe in a multiferroic heterostructure. We develop a model describing the magnetization distribution in the ferromagnetic material, properly taking into account the magnetoelectric coupling. Through its numerical implementation, we obtain the relationship between the electric field applied to the piezoelectric substrate and the position of the magnetic domain wall in the nanostripe. As an example, we analyze a structure composed of a PMN-PT substrate and a $TbCo_2$/FeCo composite nanostripe. © *2016 AIP Publishing LLC*. [http://dx.doi.org/10.1063/1.4942388]

Magnetic domain wall control in nanoscale structures is a promising subject for magnetic logic[1] and memory devices.[2] The domain wall propagation is typically induced by external magnetic fields,[3–5] spin-polarized currents,[6–9] localized non-uniform mechanical stress,[10–12] pinning onto ferroelectric domain walls,[13,14] and temperature gradients.[15] Also, the mobility of a current-induced domain wall can be piezoelectrically controlled through a strain-mediated magnetic anisotropy.[16] Theoretical and experimental studies of concept devices based on magnetic domain walls range from neuromorphic systems,[17] spintronic logic,[18] racetrack memories,[19] memristors,[20] to lab-on-chip manipulation of magnetic microbeads.[21]

Here, we propose the analysis of the domain wall displacement induced by uniform mechanical stress in a nanostripe with variable section. We introduce an external magnetic field to break the symmetry of the two stable states of magnetization in a uniaxial ferromagnet. When applying the uniform stress to the two-domain system, the wall moves so as to expand the domain that is energetically favored and contract the other one. Since the stress can be generated by a piezoelectric substrate, the system belongs to the class of multiferroic heterostructures.[22] The idea of breaking the symmetry of states has been largely exploited to design memory elements[23–25] and is here generalized to systems with analog behavior. The switching process between two states of a single domain element is thus replaced by a continuous wall motion between two adjacent domains. It has been proved that the stress-mediated control of magnetization allows for excellent energy efficiency.[26–28] Accordingly, the scheme hereby proposed is a relevant alternative to current and magnetic field based domain wall motion techniques, which are subject to higher energy consumption.

The proposed system is shown in Fig. 1. The nanostripe geometry is described by the region $V = \{-\frac{L}{2} \le x \le \frac{L}{2}, -\frac{\ell(x)}{2} \le y \le \frac{\ell(x)}{2}, -\frac{h}{2} \le z \le \frac{h}{2}\}$, exhibiting a variable cross-section $h\ell(x)$. External magnetic and electric fields $\vec{H}_0$ and $\vec{E}_0$ are applied to the system. The perpendicular electric field activates the substrate, thus generating the planar stress components σ and τ shown in Fig. 1. By considering a piezoelectric material with coefficients $d_{32} > 0$ and $d_{31} < 0$ (as, e.g., in PMN-PT[29]), we obtain $\sigma > 0$ and $\tau < 0$ when $E_0 > 0$, and $\sigma < 0$ and $\tau > 0$ when $E_0 < 0$. The magnetization distribution in V is defined by $\vec{M}(\vec{r}) = M_s\vec{\gamma}(\vec{r})$, where M_S represents the magnetization at saturation and $\vec{\gamma}$ is a unit vector. We further assume that the magnetization remains in the (x, y) plane and only depends on variable x. Therefore, $\vec{M}(\vec{r}) = M_S(\cos\theta(x), \sin\theta(x), 0)$, where $\theta(x)$ is the angle formed by $\vec{M}$ with respect to the x-axis (see Fig. 1).

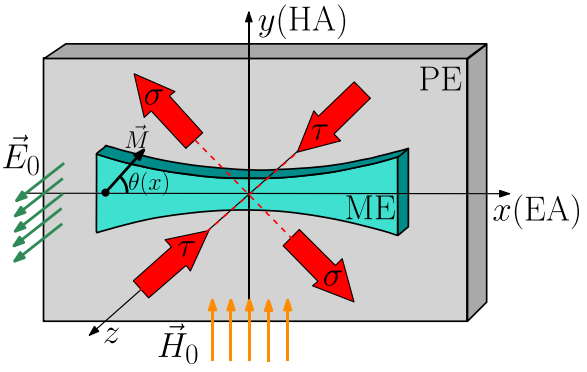

FIG. 1. Multiferroic heterostructure composed of a piezoelectric (PE) substrate and a magnetoelastic (ME) layer. The ferromagnetic easy-axis (EA) is aligned with the x-axis, while the hard-axis (HA) corresponds to the y-axis. The magnetization $\vec{M}$ is described by the angle $\theta(x)$. The magnetic field $\vec{H}_0 = H_0\vec{e}_y$ and the electric field $\vec{E}_0 = E_0\vec{e}_z$ are applied to the system. The field $\vec{E}_0$ produces stress components σ and τ on the plane.

a)Electronic mail: Stefano.Giordano@iemn.univ-lille1.fr

To introduce the working principle of the proposed concept device, we define the total energy of the system (minimum at equilibrium) as the sum of anisotropic, exchange, Zeeman, magnetoelastic, and demagnetization terms (see below for their definitions). We initially suppose that $\vec{H}_0 = 0$ and $\vec{E}_0 = 0$. In these conditions, we consider a Néel domain wall, positioned at $x = 0$, between two regions with uniform magnetizations $\vec{M}_1$ and $\vec{M}_2$ (opposite states coming from the uniaxial anisotropy, see Fig. 2). When the magnetic field $\vec{H}_0 \neq 0$ is applied (perpendicularly to the easy-axis), $\vec{M}_1$ and $\vec{M}_2$ change to $\vec{M}_1'$ and $\vec{M}_2'$, which are tilted but still symmetric with respect to the y-axis. Again, the energy is minimum with the domain wall at $x = 0$ since the energy density is the same in the two domains. If $\vec{E}_0 \neq 0$ is then applied, the new states $\vec{M}_1''$ and $\vec{M}_2''$ lose the symmetry (see Fig. 2). Therefore, the domain wall moves so as to reduce the size of the domain with higher energy density in order for the system to attain equilibrium. Note that the stress is capable of breaking the symmetry only if $\vec{H}_0 \neq 0$, which is therefore a crucial element of the system. Indeed, if the stress is applied to the system with $\vec{H}_0 = 0$, the magnetic states are tilted but still opposite so that the energy density is again the same in the two domains, precluding motion. The geometry with larger section close to the extremities guarantees the existence of an equilibrium position for the domain wall, preventing it from reaching the extremities and thus being ejected. Indeed, the domain wall has an intrinsic surface energy (proportional to the wall area), which participates to the total system energy. Simple analytical expressions of the wall surface energy are reported in classical textbooks in terms of exchange and anisotropy coefficients.[30] However, these approaches neglect other important contributions (external fields, magnetoelasticity, demagnetization) addressed in the following model, which provides a clear understanding of the underlying physics without the computational effort required by micromagnetic simulations.

From the point of view of the physical response of the ferromagnetic material, the uniaxial behavior along the x-axis is described by the anisotropic energy density[30,31]

$$u_{an} = -K_u \gamma_x^2 = -K_u \cos^2\theta, \tag{1}$$

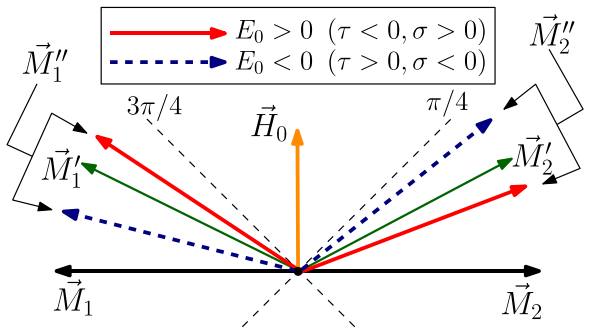

FIG. 2. Stable states of magnetization. The uniaxial anisotropy, without external fields, induces two opposite states $\vec{M}_1$ and $\vec{M}_2$. When $\vec{H}_0$ is applied, their angle is modified, by obtaining $\vec{M}_1'$ and $\vec{M}_2'$, still symmetric. Further, the mechanical stress leads to the tilted states $\vec{M}_1''$ and $\vec{M}_2''$, which are asymmetric for both $E_0 > 0$ and $E_0 < 0$.

where K_u is the anisotropy constant. Similarly, the exchange interaction must be introduced through the energetic contribution $u_{ex} = \frac{1}{2}\alpha_{ij}\frac{\partial \gamma_l}{\partial x_i}\frac{\partial \gamma_l}{\partial x_j}$, where α_{ij} is a symmetric tensor.[30] Coherently with the uniaxial symmetry, we have that $\alpha_{11} = 2A$, $\alpha_{22} = \alpha_{33} = 2B$, and $\alpha_{ij} = 0\ \forall\, i \neq j$. With previous assumptions on $\vec{M}(\vec{r})$, we easily get

$$u_{ex} = A\left(\frac{\mathrm{d}\theta}{\mathrm{d}x}\right)^2. \tag{2}$$

The external magnetic field, applied along the y-axis, leads to the Zeeman energetic contribution[30,31]

$$u_{Ze} = -\mu_0 M_S \vec{H}_0 \cdot \vec{\gamma} = -\mu_0 M_S H_0 \sin\theta. \tag{3}$$

The general form of the energy density describing the magnetoelastic interaction is $u_{me} = -T_{ij}\epsilon_{ij}^{\mu}$, where T_{ij} is the local Cauchy stress tensor and $\epsilon_{ij}^{\mu}(\vec{\gamma})$ is the strain characterizing the magnetostrictive effect.[32] Its mathematical form is $\epsilon_{ij}^{\mu} = \frac{\lambda_S}{2}\left(3\gamma_i\gamma_j - \delta_{ij}\right)$, where λ_S is the magnetostriction coefficient. As an example, if $T_{11} = \tau$ and $T_{22} = \sigma$ and the other stress components are zero, we obtain $u_{me} = -\frac{3}{2}\lambda_S(\sigma - \tau)\gamma_2^2 + const.$ Now, within the piezoelectric material we have the strains $\epsilon_{11} = d_{31}E_0$ and $\epsilon_{22} = d_{32}E_0$. On the other hand, in the magnetoelastic material we have $T_{ij} = 2\mu\epsilon_{ij} + \lambda\epsilon_{kk}$, where λ and μ are the Lamé coefficients. By considering $T_{33} = 0$ and ϵ_{11} and ϵ_{22} imposed by the piezoelectric substrate, we easily obtain $T_{11} = \tau = 2\mu\frac{2(\lambda+\mu)d_{31}+\lambda d_{32}}{2\mu+\lambda}E_0$ and $T_{22} = \sigma = 2\mu\frac{2(\lambda+\mu)d_{32}+\lambda d_{31}}{2\mu+\lambda}E_0$. The corresponding energy density is therefore given by $u_{me} = -3\lambda_S\mu E_0(d_{32} - d_{31})\gamma_2^2 + const.$ In our case, the piezoelectric substrate is rotated by an angle of $\pi/4$ with respect to the frame (x, y), as shown in Fig. 1. Therefore, we must substitute $\gamma_2^2 = \sin^2(\theta - \frac{\pi}{4}) = -\sin\theta\cos\theta + const.$, to eventually obtain

$$u_{me} = 3\lambda_S\mu E_0(d_{32} - d_{31})\sin\theta\cos\theta. \tag{4}$$

For instance, if we use the piezoelectric [011] cut PMN-PT ceramic (near the so-called morphotropic phase boundary), we have $d_{32} = 1000\,\mathrm{pC/N}$ and $d_{31} = -1900\,\mathrm{pC/N}$,[29] assuring a strong magnetoelectric coupling. To sum up, the total energy of the system is

$$\begin{aligned} U = \int_{-\frac{L}{2}}^{\frac{L}{2}} h\ell(x)\Bigg[&-K_u\cos^2\theta + A\left(\frac{\mathrm{d}\theta}{\mathrm{d}x}\right)^2 \\ &-\mu_0 M_S H_0\sin\theta + 3\lambda_S\mu E_0(d_{32} - d_{31})\sin\theta\cos\theta\Bigg]\mathrm{d}x \\ &-\frac{1}{2}\mu_0 M_S^2\int_V\int_V \vec{\gamma}(\vec{r})\cdot\overleftrightarrow{N}(\vec{r},\vec{r}_0)\vec{\gamma}(\vec{r}_0)\,\mathrm{d}\vec{r}_0\mathrm{d}\vec{r}, \end{aligned} \tag{5}$$

where the last term represents the demagnetization energy density,[30–32] which is based on the demagnetization tensor

$$\overleftrightarrow{N}(\vec{r},\vec{r}_0) = \frac{1}{4\pi}\left[\frac{3(\vec{r}-\vec{r}_0)\otimes(\vec{r}-\vec{r}_0)}{\|\vec{r}-\vec{r}_0\|^5} - \frac{\overleftrightarrow{I}}{\|\vec{r}-\vec{r}_0\|^3}\right], \tag{6}$$

used to determine the demagnetization field $\vec{H}_d(\vec{r}) = M_S \int_V \overleftrightarrow{N}(\vec{r},\vec{r_0})\vec{\gamma}(\vec{r_0})\mathrm{d}\vec{r_0}$.[33] In Eq. (6), $(\vec{a}\otimes\vec{b})_{ij} = a_i b_j$ represents the tensor product of vectors, and $\overleftrightarrow{I}$ is the identity operator.

The actual magnetization distribution within V can be found by minimizing U with respect to the function $\theta(x)$. This is a problem of the calculus of variations[34] and it can be addressed by imposing that $\frac{\mathrm{d}}{\mathrm{d}\alpha} U[\theta(x)+\alpha k(x)]|_{\alpha=0} = 0\,\forall k(x)$ (with $k(\pm L/2) = 0$), where the left hand side corresponds to the Gâteaux derivative of U.[35] A long analytical development, exploiting the symmetries $\overleftrightarrow{N}(\vec{r},\vec{r_0}) = \overleftrightarrow{N}^{T}(\vec{r},\vec{r_0})$ and $\overleftrightarrow{N}(\vec{r},\vec{r_0}) = \overleftrightarrow{N}(\vec{r_0},\vec{r})$ of $\overleftrightarrow{N}$, yields the equation

$$\frac{\mathrm{d}^2\theta}{\mathrm{d}x^2} + \frac{\mathrm{d}\theta}{\mathrm{d}x}\frac{1}{\ell}\frac{\mathrm{d}\ell}{\mathrm{d}x} - \frac{K_u}{2A}\left[\sin(2\theta) - \xi\cos\theta + \eta\cos(2\theta) + \frac{\mu_0 M_S}{K_u}\left(\sin\theta\langle H_{d,x}\rangle_{y,z} - \cos\theta\langle H_{d,y}\rangle_{y,z}\right)\right] = 0, \tag{7}$$

where $\langle\vec{H}_d\rangle_{y,z}(x) = \frac{1}{h\ell(x)}\int_{-\frac{\ell(x)}{2}}^{+\frac{\ell(x)}{2}}\int_{-\frac{h}{2}}^{+\frac{h}{2}}\vec{H}_d(\vec{r})\,\mathrm{d}z\mathrm{d}y$ represents the average value of the demagnetization field over the nanostripe section, and the adimensional parameters $\xi = \frac{\mu_0 M_s H_0}{K_u}$ and $\eta = \frac{3\lambda_s\mu E_0(d_{32}-d_{31})}{K_u}$ measure the intensity of the applied magnetic field and mechanical stress (or electric field), respectively. Since we wish to study the displacement of the domain wall within $\left[-\frac{L}{2},+\frac{L}{2}\right]$, we fix the values $\theta\left(-\frac{L}{2}\right)$ and $\theta\left(+\frac{L}{2}\right)$ consistently with the states $\vec{M}_1''$ and $\vec{M}_2''$, defined in Fig. 2 and corresponding to the solutions of $\sin(2\theta) - \xi\cos\theta + \eta\cos(2\theta) = 0$. Since $\langle\vec{H}_d\rangle_{y,z}$ depends on $\theta(x)$, the result stated in Eq. (7) represents a second order integro-differential equation with boundary conditions. To solve this boundary value problem, we developed an *ad hoc* nonlinear iterative method,[36] combined with an efficient determination of the demagnetization field. To compute the latter, we partition the region V along the x-axis in a given number of parallelepipeds of variable size, consistently with the shape function $\ell(x)$. Since the field produced by a uniformly magnetized parallelepiped can be exactly calculated through closed form expressions,[37] we can add all the contributions to get $\vec{H}_d$ and its average $\langle\vec{H}_d\rangle_{y,z}$.

In Fig. 3, we show the solution of Eq. (7) for a $TbCo_2$/FeCo composite nanostripe, obtained by considering $M_s = 64\times10^4$ A/m, $A = 9\times10^{-12}$ J/m, and $K_u = 37.5\times10^3$ J/m^3. By writing the anisotropy constant as $K_u = \frac{1}{2}\mu_0 M_s H_a$, we can identify the effective anisotropy field $H_a = 92\times10^3$ A/m, which can be easily obtained in real ferromagnetic layers.[24] We explored the interval $-3.5 \le \eta \le +3.5$, which means that $-10^6\,\mathrm{V/m} \le E_0 \le 10^6\,\mathrm{V/m}$ if we suppose that $\lambda_s = 2\times10^{-4}$, $\mu = 80$ GPa, and the piezoelectric coefficients correspond to the PMN-PT ceramic.[29] Moreover, we imposed the value $\xi = 0.43$, corresponding to an applied magnetic field $H_0 = 20\times10^3$ A/m. This can be simply implemented using patterned nanomagnets.[38] Concerning the geometry of the nanostripe, we considered $L = 400$ nm, $h = 20$ nm, and a quadratic shape function $\ell(x) = a + \frac{4(b-a)}{L^2}x^2$, where

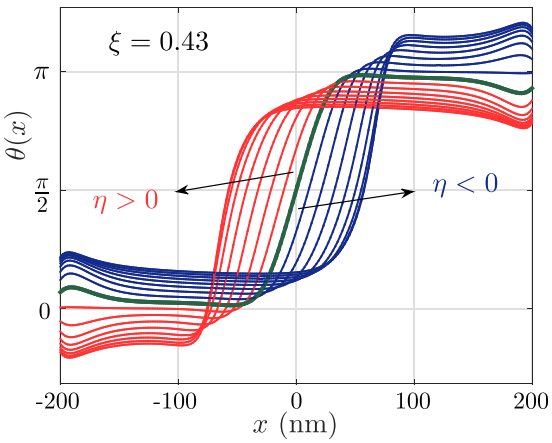

FIG. 3. Magnetization orientation distributions $\theta(x)$ within the nanostripe for a fixed magnetic field (fixed ξ) and several values of electric field (17 values of η uniformly distributed in $-3.5 \le \eta \le +3.5$). We observe that the domain wall moves to the left for $\eta > 0$ and to the right for $\eta < 0$.

$a = l(0) = 40$ nm (central width) and $b = l(\pm L/2) = 80$ nm (width at extremities). In Fig. 3, we can observe that the domain wall moves leftward for $\eta > 0$ and rightward for $\eta < 0$, expanding the favored domain and contracting the other one. Besides, this behavior is reversible with respect to the values of η. We can identify, for the example under consideration, a maximum displacement as large as $x_{p,max} = 70$ nm in both left and right directions.

The result in Fig. 3 can be used to determine the position of the domain wall in terms of the parameter η ($-4.5 < \eta < +4.5$). This is shown in Fig. 4 for three different profiles of the nanostripe: $\ell_1(x)$ corresponds to the shape used in Fig. 3, $\ell_2(x)$ to the same function with $a = 40$ nm and $b = 90$ nm, and $\ell_3(x)$ to $a = 40$ nm and $b = 100$ nm. Interestingly enough, a larger section at the extremities of the nanostripe reduces the maximum displacement of the domain wall. Moreover, there is a threshold value for $b - a$ under which it is not possible to stabilize the position of the wall for a given stress. In fact, we proved that Eq. (7) with constant $\ell(x)$ has solutions showing the wall ejection when the stress is applied. This substantiates the design of the

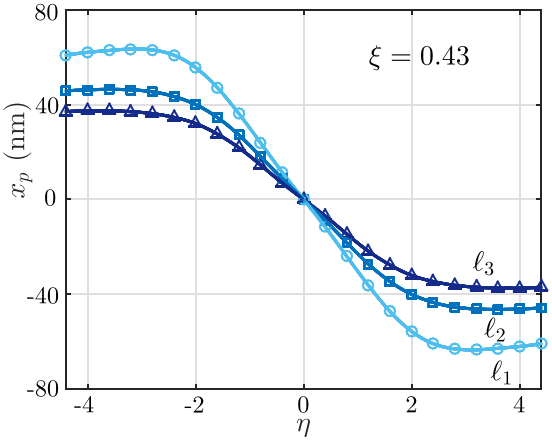

FIG. 4. Displacement x_p of the Néel domain wall in the magnetic nanostripe versus the parameter η quantifying the applied electric field ($-4.5 < \eta < +4.5$). The curves correspond to three different quadratic functions $\ell_1(x)$ (circles), $\ell_2(x)$ (squares), and $\ell_3(x)$ (triangles).

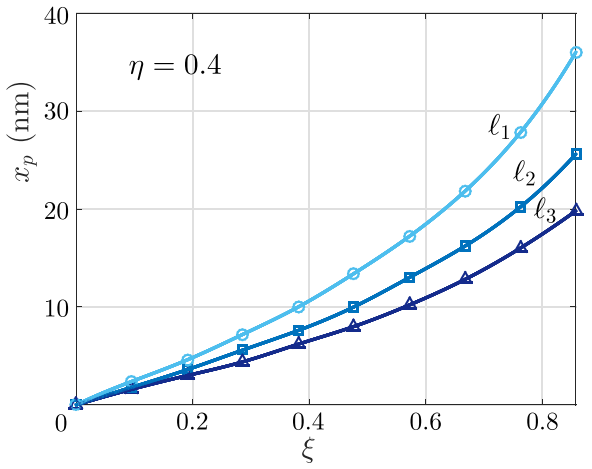

FIG. 5. Effect of the external magnetic field (quantified by ξ) on the displacement of the domain wall for three different shapes ℓ_1, ℓ_2, and ℓ_3 of the nanostripe and for a fixed mechanical stress or electric field (quantified by η).

nanostripe with a variable cross-section, increasing toward the extremities. These results have been confirmed by standard micromagnetic simulations, not reported here for the sake of brevity. All cases shown in Fig. 4 exhibit a nearly linear region for low values of the electric field, a maximum displacement for a given η, and an inversion of the direction of motion by further increasing η. Of course, it is the energetic difference between the domains (total energy without the exchange contribution) that directly drives the extent of the displacement of the domain wall. Now, if we consider only anisotropic, magnetoelastic, and Zeeman contributions, this difference exhibits a saturation trend for large values of η. Then, it is the complex behavior of the demagnetization energy that explains the inversion of the direction of motion for large values of η. Finally, in Fig. 5 we analyze the effect of the static magnetic field on the displacement of the domain wall. As expected, the displacement is an increasing function of the magnetic field intensity (with a fixed electric field). Nevertheless, there are two different magnetization states only for magnetic fields below a given threshold. For instance, when $\eta = 0$, there are two distinct orientations (given by $\sin(2\theta) - \xi \cos\theta = 0$) only if $|\xi| < 2$. We also underline that in our model we neglected possible pinning effects, which can yield an hysteretic response, depending on density and size of defects or imperfections.

To conclude, we theoretically demonstrated the possibility to control a magnetic domain wall position in a multiferroic heterostructure. This technique is relevant from the energetic point of view. Indeed, if we consider a piezoelectric PMN-PT substrate (length $L = 400\,\text{nm}$, width $b = 80\,\text{nm}$, and thickness $d = 1\,\mu\,\text{m}$) with relative dielectric constant $\varepsilon_r = 5500$ for the structure described by $\ell_1(x)$, we obtain an energy $\Delta E = \varepsilon_r \varepsilon_0 L b d E_0^2 = 1.5\,\text{fJ} = 3.6 \times 10^5 k_B T$ for moving the wall between $-x_{p,max}$ and $x_{p,max}$ (we used $E_0 = \pm 10^6\,\text{V/m}$ generated by an electric potential difference of $\pm 1\,\text{V}$). For comparison, we can cite the energy dissipation $\Delta E = 10^4\,\text{fJ}$ for one logic operation in a current-driven gate based on the domain wall motion.[39] Further investigations on this subject will consist in analyzing the dynamic behavior,[31] the effects of thermal noise,[40] and the response of a real prototype.

[1]D. A. Allwood, G. Xiong, C. Faulkner, D. Atkinson, D. Petit, and R. P. Cowburn, Science **309**, 1688 (2005).
[2]S. S. Parkin, M. Hayashi, and L. Thomas, Science **320**, 190 (2008).
[3]T. Ono, H. Miyajima, K. Shigeto, K. Mibu, N. Hosoito, and T. Shinjo, Science **284**, 468 (1999).
[4]D. Atkinson, D. A. Allwood, G. Xiong, M. D. Cooke, C. C. Faulkner, and R. P. Cowburn, Nat. Mater. **2**, 85 (2003).
[5]G. S. D. Beach, C. Nistor, C. Knutson, M. Tsoi, and J. L. Erskine, Nat. Mater. **4**, 741 (2005).
[6]M. Hayashi, L. Thomas, C. Rettner, R. Moriya, Y. B. Bazaliy, and S. S. P. Parkin, Phys. Rev. Lett. **98**, 037204 (2007).
[7]D. Ravelosona, S. Mangin, J. A. Katine, E. E. Fullerton, and B. D. Terris, Appl. Phys. Lett. **90**, 072508 (2007).
[8]A. V. Khvalkovskiy, V. Cros, D. Apalkov, V. Nikitin, M. Krounbi, K. A. Zvezdin, A. Anane, J. Grollier, and A. Fert, Phys. Rev. B **87**, 020402 (2013).
[9]P. N. Skirdkov, K. A. Zvezdin, A. D. Belanovsky, J. Grollier, V. Cros, C. A. Ross, and A. K. Zvezdin, Appl. Phys. Lett. **104**, 242401 (2014).
[10]J. Dean, M. T. Bryan, T. Schrefl, and D. A. Allwood, J. Appl. Phys. **109**, 023915 (2011).
[11]M. T. Bryan, J. Dean, and D. A. Allwood, Phys. Rev. B **85**, 144411 (2012).
[12]N. Lei, T. Devolder, G. Agnus, P. Aubert, L. Daniel, J.-V. Kim, W. Zhao, T. Trypiniotis, R. P. Cowburn, C. Chappert, D. Ravelosona, and P. Lecoeur, Nat. Commun. **4**, 1378 (2013).
[13]B. Van de Wiele, L. Laurson, K. J. A. Franke, and S. van Dijken, Appl. Phys. Lett. **104**, 012401 (2014).
[14]K. J. A. Franke, B. Van de Wiele, Y. Shirahata, S. J. Hämäläinen, T. Taniyama, and S. van Dijken, Phys. Rev. X **5**, 011010 (2015).
[15]R. Tolley, T. Liu, Y. Xu, S. Le Gall, M. Gottwald, T. Hauet, M. Hehn, F. Montaigne, E. E. Fullerton, and S. Mangin, Appl. Phys. Lett. **106**, 242403 (2015).
[16]E. De Ranieri, P. E. Roy, D. Fang, E. K. Vehsthedt, A. C. Irvine, D. Heiss, A. Casiraghi, R. P. Campion, B. L. Gallagher, T. Jungwirth, and J. Wunderlich, Nat. Mater. **12**, 808 (2013).
[17]M. Sharad, C. Augustine, G. Panagopoulos, and K. Roy, IEEE Trans. Nanotechnol. **11**, 843 (2012).
[18]B. Behin-Aein, D. Datta, S. Salahuddin, and S. Datta, Nat. Nanotechnol. **5**, 266 (2010).
[19]S. Parkin and S.-H. Yang, Nat. Nanotechnol. **10**, 195 (2015).
[20]N. Locatelli, V. Cros, and J. Grollier, Nat. Mater. **13**, 11 (2014).
[21]H. Sohn, M. E. Nowakowski, C. Y. Liang, J. L. Hockel, K. Wetzlar, S. Keller, B. M. McLellan, M. A. Marcus, A. Doran, A. Young, M. Kläui, G. P. Carman, J. Bokor, and R. N. Candler, ACS Nano **9**, 4814 (2015).
[22]C. W. Nan, M. I. Bichurin, S. Dong, D. Viehland, and G. Srinivasan, J. Appl. Phys. **103**, 031101 (2008).
[23]N. Tiercelin, Y. Dusch, V. Preobrazhensky, and P. Pernod, J. Appl. Phys. **109**, 07D726 (2011).
[24]N. Tiercelin, Y. Dusch, A. Klimov, S. Giordano, V. Preobrazhensky, and P. Pernod, Appl. Phys. Lett. **99**, 192507 (2011).
[25]A. K. Biswas, S. Bandyopadhyay, and J. Atulasimha, Appl. Phys. Lett. **104**, 232403 (2014).
[26]S. Giordano, Y. Dusch, N. Tiercelin, P. Pernod, and V. Preobrazhensky, Phys. Rev. B **85**, 155321 (2012).
[27]S. Giordano, Y. Dusch, N. Tiercelin, P. Pernod, and V. Preobrazhensky, J. Phys. D: Appl. Phys. **46**, 325002 (2013).
[28]K. Roy, S. Bandyopadhyay, and J. Atulasimha, J. Appl. Phys. **112**, 023914 (2012).
[29]Y. Dusch, N. Tiercelin, A. Klimov, S. Giordano, V. Preobrazhensky, and P. Pernod, J. Appl. Phys. **113**, 17C719 (2013).
[30]L. D. Landau and E. M. Lifshitz, *Electrodynamics of Continuous Media* (Pergamon Press, London, 1984).
[31]W. F. Brown, *Micromagnetics* (Interscience Publisher, New York, 1963).
[32]W. F. Brown, *Magnetoelastic Interactions* (Springer-Verlag, Berlin, 1966).
[33]J. A. Stratton, *Electromagnetic Theory* (McGraw Hill, New York, 1941).
[34]C. Miehe and G. Ethiraj, Comput. Methods Appl. Mech. Eng. **245**, 331 (2012).

[35]A. N. Kolmogorov and S. V. Fomin, *Elements of the Theory of Functions and Functional Analysis* (Dover, New York, 1999).
[36]H. B. Keller, *Numerical Solution of Two Point Boundary Value Problems* (SIAM, Philadelphia, 1976).
[37]R. Ravaud and G. Lemarquand, Prog. Electromagn. Res. B **98**, 207–219 (2009).
[38]Y. Dusch, N. Tiercelin, A. Klimov, V. Rudenko, Y. Ignatov, S. Hage-Ali, P. Pernod, and V. Preobrazhensky, J. Appl. Phys. **109**, 07A720 (2011).
[39]P. Xu, K. Xia, C. Gu, L. Tang, H. Yang, and J. Li, Nat. Nanotechnol. **3**, 97 (2008).
[40]S. Giordano, Y. Dusch, N. Tiercelin, P. Pernod, and V. Preobrazhensky, Eur. Phys. J. B **86**, 249 (2013).